Published in final edited form as:
J Med Chem. 2009 January 22; 52(2): 358–368. doi:10.1021/jm801052f.

Photodynamic Molecular Beacon Triggered by Fibroblast Activation Protein on Cancer-associated Fibroblasts for Diagnosis and Treatment of Epithelial Cancers

Pui-Chi Lo[1,2], **Juan Chen**[1,2], **Klara Stefflova**[3], **Michael S. Warren**[3], **Roya Navab**[4], **Bizhan Bandarchi**[4], **Stefanie Mullins**[5], **Ming Tsao**[1,4], **Jonathan D. Cheng**[5], and **Gang Zheng**[1,2,6]

[1] Department of Medical Biophysics, University of Toronto, Toronto, ON, M5G 1L7, Canada

[2] Division of Biophysics and Bioimaging, Ontario Cancer Institute, Toronto, ON, M5G 1L7, Canada

[3] Department of Chemistry, University of Pennsylvania, Philadelphia, PA 19104, USA

[4] Division of Applied Molecular Oncology, Ontario Cancer Institute, Toronto, ON, M5G 1L7, Canada

[5] Fox Chase Cancer Center, Department of Medical Oncology, Philadelphia, Pennsylvania 19111, USA

[6] Department of Radiology, University of Pennsylvania, Philadelphia, PA 19104, USA

Abstract

Fibroblast activation protein (FAP) is a cell-surface serine protease highly expressed on cancer-associated fibroblasts of human epithelial carcinomas but not on normal fibroblasts, normal tissues, and cancer cells. We report herein a novel FAP-triggered photodynamic molecular beacon (FAP-PPB) comprising of a fluorescent photosensitizer and a black hole quencher 3 linked by a peptide sequence (TSGPNQEQK) specific to FAP. FAP-PPB was effectively cleaved by both human FAP and murine FAP. Using the HEK293 transfected cells (HEK-mFAP, FAP^+; HEK-Vector, FAP^-), systematic in vitro and in vivo experiments validated the FAP-specific activation of FAP-PPB in cancer cells and mouse xenografts, respectively. FAP-PPB was cleaved by FAP, allowing fluorescence restoration in FAP-expressing cells, while leaving non-expressing FAP cells undetectable. Moreover, FAP-PPB showed FAP-specific photocytotoxicity toward HEK-mFAP cells whereas it was non-cytotoxic toward HEK-Vector cells. This study suggests that the FAP-PPB is a potentially useful tool for epithelial cancer detection and treatment.

Keywords

Fibroblast Activation Protein (FAP); Cancer-associated Fibroblast (CAF); Molecular Beacon; In Vivo Imaging; Photodynamic Therapy (PDT)

Correspondence addressed to: Dr. Gang Zheng, MaRS Center, TMDT 5-363, 101 College St., Toronto, ON, M5G 1L7, Canada, gang.zheng@uhnres.utoronto.ca, phone: 416-581-7666, fax: 416-581-7667.

Supporting Information Available: Characterization of 2D-FAP-PPB; Comparison of the fluorescence intensity of FAP-PP with different concentrations of free BHQ3 and the intact FAP-PPB in DMSO and buffer solution; Stern-Volmer plots for FAP-PP with different concentrations of free BHQ3 in DMSO and buffer solution; Stability of FAP-PPB toward DPPIV; Stability of FAP-PPB toward MMPs. The material is available free of charge via the Internet at http://pubs.acs.org.

Introduction

Desmoplasia is stromal fibroblastic proliferation, which commonly contributes approximately 20–50% of the tumor mass.[1, 2] This reactive stroma includes inflammatory cells, blood vessels, extracellular matrix, connective tissues, and proliferating stromal fibroblasts.[3, 4] The latter, also called cancer-associated fibroblasts (CAFs), play a critical role in the tumor microenvironment by providing growth factors and proteases contributing to tumor initiation, invasion, and metastasis.[5–7] To understand the actual functions of CAFs, a series of studies comparing the effect of normal fibroblasts and CAFs have been carried out in different animal models.[8, 9] It was revealed that while the function of normal fibroblasts is to maintain epithelial homeostasis, CAFs could initiate and promote tumorigenic transformation of epithelial cells. CAFs may also communicate by autocrine mechanism with cancer cells, resident epithelial cells, and inflammatory cells through the secreted growth factors and chemokines.[5] Although the mechanisms and functions of CAFs are not fully understood, they are promising therapeutic targets in cancer. A highly consistent and specific characteristic of CAFs is the induction of fibroblast activation protein.

Fibroblast activation protein (FAP), which is a cell surface glycoprotein belonging to the serine protease family, is expressed by the CAFs in over 90% of human epithelial cancers including breast, ovarian, bladder, colorectal, and lung cancers, but it is not expressed in epithelial cancer cells, normal fibroblasts, and other normal tissues, except the transient expression in healing wounds.[10–12] FAP exhibits both gelatinese and collagenase activities capable of degrading gelatin and unwound or denatured type I collagen, respectively.[13–15] In addition, it acts as a post-prolyl peptidase such as dipeptidyl peptidase IV (DPPIV) that can cleave N-terminal dipeptides with penultimate proline.[13, 16] It also functions as an endopeptidase that can break the Pro-Asn bond of α_2-antiplasmin and peptide substrates.[17–19] FAP plays an important role in tumor growth and metastasis as its expression on CAFs may create an environment permissive for cancer growth and invasion via collagenase and dipeptidyl peptidase activities.[16, 20–23] Because FAP expression has been consistently reported in more than 90% of all epithelial carcinoma and tumor stroma should be rich in FAP, FAP has emerged as an important biomarker and potential therapeutic target for the detection and treatment of epithelial cancers.

Several phase I trials and a limited phase II trial have been conducted using an unconjugated sibrotuzumab, which is a humanized version of the murine anti-FAP monoclonal antibody (mAb) F19.[24–26] Sibrotuzumab was well-tolerated and safe for patients with advanced FAP-expressing cancers. An imaging study in colorectal carcinoma and non-small cell lung carcinoma patients using the ^{131}iodine-labelled sibrotuzumab has revealed that sibrotuzumab specifically accumulated in tumors, but not in normal tissues after 24–48 h administration. Although safe administration has been shown, no clinical tumor responses have been observed by treatment with this unconjugated mAb, and the antibodies did not inhibit FAP enzymatic activity. It remains plausible that FAP-specific reagents such as sibrotuzumab conjugated to toxic agents may effectively target and kill tumors while sparing normal tissues. More recently, the small molecule inhibitor of FAP, Val-boro-Pro (called talabostat or PT-100), has been shown to attenuate and inhibit tumor growth in a variety of tumor models in mice.[23, 27] Clinical phase II trials using talabostat with or without chemotherapy in stage IV melanoma patients demonstrated clinical responses.[28–30] However, similar phase II trial in metastatic colorectal cancer patients showed only minimal clinical activity.[31]

Our group has recently introduced photodynamic molecular beacons which is comprised of a disease-specific linker, a photosensitizer (PS), and a fluorescence and singlet oxygen ($^1O_2$) quencher (Q).[32, 33] The intact photodynamic molecular beacons are non-fluorescent and non-cytotoxic because of energy transfer from the excited PS to Q. Upon activation by the target molecule (e.g. tumor-specific protease), the linker will be cleaved which allows the separation

of PS and Q. Upon irradiation, this leads to fluorescence emission restoration and $^1O_2$ generation. Therefore, photodynamic molecular beacons offer a control of fluorescence emission and $^1O_2$ generation of PS in response to specific cancer target activation. Based on this principle, we have designed a new photodynamic molecular beacon for the imaging and treatment of FAP-expressing cancers by targeting FAP on CAFs. The design, preparation, and functional evaluation of this beacon, as well as its in vitro and in vivo validation of FAP specificity, are reported herein.

Materials and Methods

General Materials

The activating agents 1-hydroxybenzotriazole (HOBt) and o-(benzotriazol-1-yl)-*N*,*N*,*N*′,*N*′-tetramethyluronium hexafluorophosphate (HBTU), and the black hole quencher 3 carboxylic acid succinimdyl ester (BHQ3-NHS) were received from Acros, Sigma-Aldrich, and Biosearch Technologies, respectively, and used without further purification. The Sieber amide resins and all the 9H-fluoren-9-ylmethoxycarbonyl (N-α-Fmoc)-protected amino acids were purchased from Novabiochem.

General HPLC Methods

Reverse-phase analytical HPLC experiments were performed on a XBridge™-C18 column (2.5 μM, 4.6 × 50 mm) using a Waters 2695 controller with a 2996 photodiode array detector and a Waters ZQ™ mass detector. The conditions were as follows: solvent A = acetonitrile; solvent B = 0.1% trifluoroacetic acid (TFA); gradient: from 40% A + 60% B to 50% A + 50% B in the first 5 min, then to 80% A + 20% B in 30 min and further to 100% A for 5 min, finally to 40% A + 60% B for 5 min; flow rate: 0.5 mL min^{-1}.

Synthesis of Fmoc-T(^{t}Bu)S(^{t}Bu)GPNQE(O^{t}Bu)QK(Mtt)-Sieber resin (1)

This peptide resin (100 μmol scale) was synthesized according to the Fmoc solid phase peptide synthesis (SPPS)[34] protocol using a PS3™ peptide synthesizer (Protein Technologies Inc.) with commercially available N-α-Fmoc-protected amino acids, Seiber amide resin as a solid support, and HOBt/HBTU as the carboxyl-group activating agents. A portion of **1** was treated with 95% trifluoroacetic acid (TFA), 5% triisopropylsilane (Tis), then the mixture was checked by HPLC-MS [*m/z* calcd for Fmoc-TSGPNQEQK(ε-NH_2) $C_{54}H_{76}N_{14}O_{18}$ $[M]^+$ 1209.3, found: 1209.7, purity: 98%].

Synthesis of Pyro-T(^{t}Bu)S(^{t}Bu)GPNQE(O^{t}Bu)QK(Mtt)-Sieber resin (2)

The pyropheophorbide *a* acid (Pyro) was prepared according to literature procedure.[35] After the last Fmoc group had been removed from the peptide-resin **1** with 20% piperidine in DMF, the resin was washed with DMF. Pyro was then added to couple to the N-terminal threonine of the peptide-resin with the aid of HOBt and HBTU (Pyro/HOBt/HBTU/peptide = 3:3:3:1 mole ratio). The mixture was shaken under argon overnight at room temperature. The dark green resin was washed with DMF and CH_2Cl_2 followed by drying in vacuum. A portion of 2 was treated with 95% TFA, 5% Tis. After removing the solid support by filtration, the filtrate was injected to HPLC to validate that the Pyro coupling efficiency is over 95%.

Synthesis of Pyro-T(^{t}Bu)S(^{t}Bu)GPNQE(O^{t}Bu)QK(ε-NH_2) (3)

The peptide resin **2** was treated with 3% TFA (30 μL) and 5% Tis (50 μL) in anhydrous CH_2Cl_2 (920 μL) for 1 h at room temperature to deprotect the methyltrityl (Mtt) group on the C-terminal of lysine and cleave the peptide sequence from the Sieber resin. After removing the solid resin by filtration, the filtrate was concentrated and precipitated by adding anhydrous

diethyl ether to give **3**, which was further washed with diethyl ether and dried under reduced pressure (*m/z* calcd for $C_{84}H_{122}N_{18}O_{18}$ $[M]^+$ 1672.0, found: 1672.2).

Synthesis of Pyro-TSGPNQEQK(BHQ3) (FAP-PPB)

The pyro-peptide **3** (16.7 mg, 10 μmol) was dissolved in 200 μL of anhydrous DMSO with 1% of *N*,*N*-diisopropylethylamine (DIPEA). The mixture was treated with BHQ3 carboxylic acid succinimidyl ester (BHQ3-NHS) (10.3 mg, 13 μmol) at ambient temperature for 6 h under argon. The reaction was quenched by precipitation with diethyl ether (2 mL) to give Pyro-T(^{t}Bu)S(^{t}Bu)GPNQE(O^{t}Bu)QK(BHQ3). This peptide was then treated with 95% TFA (950 μL) and 5% Tis (50 μL) to remove the butyl-protected groups on threonine, serine, and glutamic acid. The mixture was then purified by HPLC to obtain pure FAP-PPB, which was characterized with UV-Vis and ESI mass spectroscopy (*m/z* calcd for $C_{105}H_{131}N_{24}O_{19}$ $[M]^+$ 2033.3, found: 1016.9 $[M]^{2+}$).

Synthesis of Pyro-TSGPNQEQK (FAP-PP)

A portion of 3 (1 μmol) was treated by 95% TFA (950 μL) and 5% Tis (50 μL) to remove all the butyl-protected groups. The mixture was then purified by HPLC to give pure FAP-PP as positive control, which only contained Pyro fluorophore and peptide sequence (without the quencher) (*m/z* calcd for $C_{72}H_{98}N_{18}O_{18}$ $[M]^+$ 1503.7, found: 1503.3).

Synthesis of Pyro-TSGpnQEQK(BHQ3) (2D-FAP-PPB)

A peptide of Fmoc-T(^{t}Bu)S(^{t}Bu)GpnQE(O^{t}Bu)QK(Mtt)-Sieber resin (**4**) was synthesized following the same procedure as above, except that a longer coupling reaction time (3 h) was used for the D-amino acids. It was used as the FAP non-cleavable control, in which the amino acids at the cleavage site (Pro and Asn) were replaced with the corresponding D-amino acids to resist the FAP-specific cleavage. Each step of the reaction was checked by HPLC. The conjugations of Pyro and BHQ3-NHS were performed according to the above procedure (*m/z* calcd for $C_{105}H_{131}N_{24}O_{19}$ $[M]^+$ 2033.3, found: 1017.2 $[M]^{2+}$).

Quenching Efficiency Measurements

Solutions of FAP-PPB, FAP-PP, or a mixture of FAP-PP with different concentrations of BHQ3 were prepared in DMSO at a concentration of 1 μM. Their UV-Vis and fluorescence spectra were measured and compared using a Varian Cary 50 UV-Vis spectrophotometer and a HORIBA FluoroMax®-4 spectrofluorometer, respectively. To eliminate the inner filter effects, the fluorescence intensities were corrected by the equation: [36]

$$F_{corr}=F_{obs}\ \text{antilog}[(OD_{ex}+OD_{em})/2]$$

where F_{corr} and F_{obs} are the corrected and observed fluorescence, and OD_{ex} and OD_{em} correspond to the absorbance at the excitation and emission wavelengths, respectively. Their quenching efficiencies were also compared in buffer solution (0.12 M NaCl, 0.12 M TRIS, pH 7.37), in which 2.5 μL DMSO and 0.5 μL Tween 80 were used to dissolve the FAP-PPB and FAP-PP before the addition of buffer solution.

The data for FAP-PP could also be analyzed using the Stern-Volmer equation ($F_0/F = 1 + K_{SV}[Q]$), where F_0 and F are the fluorescence intensities of FAP-PP in the absence and presence of the BHQ3 quencher, respectively, [Q] is the concentration of the quencher, and K_{SV} is the Stern-Volmer quenching constant. From the slope of the Stern-Volmer plot, the corresponding Stern-Volmer quenching constant was calculated.

Activation of FAP-PPB by Human FAP and Murine FAP in Buffer

Murine FAP (mFAP) was produced and purified according to the literature procedure [22, 23] while human FAP was purchased from Biomol International LP. FAP-PPB (1 nmol) was first dissolved in 2.5 μL of DMSO and 0.5 μL of Tween 80. The solution was diluted with 1 mL of buffer solution (0.12 M NaCl, 0.12 M TRIS, pH 7.37), which was then incubated with human FAP or mFAP (2 μg) (ratio of PPB to FAP was about 50:1). The fluorescence emission of FAP-PPB was monitored in real time at 37°C by a HORIBA FluoroMax®-4 spectrofluorometer with an excitation wavelength at 650 nm and emission at 675 nm. The cleavage of 2D-FAP-PPB was also performed under the same conditions. The cleavage rate of FAP-PPB was also determined by HPLC-MS every 30 minutes until a complete cleavage was observed.

Stability of FAP-PPB toward Dipeptidyl Peptidase IV (DPPIV) and Matrix Metalloproteinases (MMPs)

FAP-PPB (1 nmol) was first dissolved in 2.5 μL of DMSO and 0.5 μL of Tween 80. It was then diluted with 1 mL of buffer solution [For MMPs: 50 mM HEPES, 10 mM $CaCl_2$, 0.5% Brij-35, pH 7 (or pH 6 for MMP3). For DPPIV: 20mM TRIS, pH 7.5]. DPPIV and MMP (purchased from Biomol International LP) were then added and it was incubated at 37 °C for 2 and 16 h, respectively (PPB: DPPIV = 228:1; PPB: MMP = 50:1). The FAP-PPB solutions were subjected to HPLC-MS analysis. The enzymatic activities of DPPIV and MMPs (including MMP 1, 2, 3, 7, 8, 9, 10, 11, 12, and 13) toward PPB were examined.

Stability of FAP-PPB in Plasma and Serum

Plasma and serum were separated from mice blood by centrifugation methods. FAP-PPB (1 nmol) was first dissolved in 2.5 μL of DMSO and 0.5 μL of Tween 80. It was then incubated with 1 mL of either serum or plasma at 37 °C over 26 h, and finally examined by HPLC.

mFAP Activity Assay

The enzymatic activity of mFAP was monitored by measuring the fluorescence emission of FAP-PPB continuously upon the addition of mFAP. Excitation and emission wavelengths of 650 nm and 675 nm, respectively, were used to monitor the liberation of Pyro fluorophore peptide cleavage fragment. Firstly, FAP-PPB (0.1, 0.3, 0.5, 0.7, 1, 2 and 6 nmol) was dissolved in 2.5 μL of DMSO and 0.5μL of Tween 80. It was then diluted with 1 mL of buffer solution (0.12 M NaCl, 0.12 M TRIS, pH 7.37) and incubated with mFAP (2 μg) at 37 °C. After 1 h, excess mFAP (10μg) was added and the mixture was monitored for a further 2 h. Assays containing different concentrations (0.1, 0.3, 0.5, 0.7, 1, 2 and 6 μM) of FAP-PPB were done in triplicate using the same amount of mFAP (2 μg). Using the initial data (10% of the substrate was depleted), kinetic parameters including maximum enzymatic rate (V_{max}), Michaelis constant (K_m), catalytic constant (k_{cat}), and k_{cat}/K_m ratio were calculated from the Michaelis-Menten plots (υ_o versus [S]) with a nonlinear regression analysis using the program SPSS (Statistical Package for the Social Sciences, version 15).

Cell Lines and Culture Conditions

The human embryonic kidney cell line HEK293 (American Type Culture Collection) was stably transfected with full-length wild-type mFAP (HEK-mFAP) and empty vector (HEK-Vector), respectively.[23] These transfected cells were maintained in Dulbecco's modified Eagle's medium (DMEM) supplemented with fetal bovine serum (FBS) (10 %), L-glutamine (2 mM), and Geneticin® (G418) (200 μg mL^{-1}) for HEK-mFAP cells (FAP^+) or hygromycin B (200 μg mL^{-1}) for HEK-Vector cells (FAP^-).

Flow Cytometric Studies

FAP-PPB (5 nmol) was first dissolved in 3.5 μL of DMSO and 0.5 μL of Tween 80. It was then diluted with the culture medium (DMEM without FBS, 0.8 mL), which had been used previously for the incubation of the cells to give a 6.25 μM FAP-PPB stock solution.

About 7×10^5 cells in the culture medium (2 mL) per well were inoculated in 6-multiwell plates and incubated for 2 days at 37°C in an atmosphere of 5% CO_2 in a humidified incubator. The medium was removed and the cells were rinsed with PBS. The cells were then incubated overnight with 1 mL of DMEM (without FBS) at 37°C under 5% CO_2. The FBS-free medium was removed and kept for the preparation of FAP-PPB solution. The cells, after being rinsed with PBS, were incubated with 0.8 mL of the FAP-PPB solution (6.25 μM) for 1, 2, 4, 6, and 24 h, respectively, at 37°C under 5% CO_2. The FAP-PPB solutions were then removed and kept for HPLC-MS measurement. The cells were then transferred to a 15 mL centrifuging tube with 2 mL of PBS. The cells were centrifuged at 1300 rpm for 6 min and the PBS was removed. This rinsing procedure was repeated for 3 times. The cells were then fixed by 2% paraformaldehyde solution for 10 min. After fixing, the cells were centrifuged and rinsed with PBS for 2 times. The fluorescence intensities of the cells were measured by a Cytomics FC 500 Series Flow Cytometry System from Beckman Coulter (excitation: 633 nm, emission: 660 – 690 nm). Autofluorescence from the untreated cells is minimal. The maximum cell number count was 10000 for all samples.

Confocal Microscopic Studies

FAP-PPB (5 nmol) and 2D-FAP-PPB (5 nmol) were first dissolved in 1.0 μL of DMSO and 0.5 μL of Tween 80. The solutions were then diluted with the culture medium (0.2 mL) previously used for cell incubation to give a 25 μM PPB solution.

About 1.5×10^4 cells in the culture medium (0.5 mL) per well were seeded in Nunc® Lab-TekII®-CC2 8-chambered slides and incubated for 2 days at 37°C under 5% CO_2. The medium (with FBS) was removed, and the cells were rinsed with PBS and incubated overnight with 0.3 mL of DMEM (without FBS) at 37°C under 5% CO_2. The FBS-free medium was removed and kept for the preparation of the above PPB solution. The cells were then incubated with 0.2 mL of the PPB solution (25 μM) for 6 h at 37°C under 5% CO_2. The PPB solution was removed and kept for HPLC-MS measurement. The cells were fixed with 3% formaldehyde in PBS (0.5 mL per well) for 20 min at dark. After fixing the cells, the chamber was removed and 10 μL of mounting solution with 4′,6-diamidino-2-phenylinodole (DAPI) (Vector Laboratories Inc.) was added to each well. The cells were finally covered by a cover slide and subjected to microscopic studies using an Olympus FluoView 1000 laser scanning confocal microscope equipped with a 405 nm diode laser and a 633 nm helium neon laser.

Mouse Xenografts and In Vivo Imaging

All animal studies were following protocols approved by the Institutional Animal Care Committee. Twelve adult Athymic female nude mice were inoculated with 1×10^7 HEK-mFAP cells (in 200 μL) and 1×10^7 HEK-Vector cells (in 200 μL) on both left and right flanks, respectively. Four nude mice were inoculated with 1×10^7 HEK-mFAP cells (in 200 μL) on both flanks. Animals were maintained in pathogen-free conditions in autoclaved microisolator cages in the MaRS Animal Resources Centre. Once the tumors were grown up (3 weeks, 5–10mm size), the mice were fed with low-fluorescence diet (Harlan Tekland) for 4 days. Mice were anesthetized with ketamine/acepromazine. PPB (25 nmol) was formulated in 30 μL aqueous solution with 2 μL of DMSO and 0.5 μL of Tween 80. Needle with 28.5 G was used for the intra-tumor injection, which was administered at different sides of tumor to improve the PPB distribution in the tumor. In vivo fluorescence imaging was performed before and after injection (at different time points) on a CRi Maestro in vivo imaging system [setting: excitation

wavelength = 650 nm, emission wavelength ≥ 700 nm, exposure time 200 ms, total fluorescence signals normalized by exposure time and ROI area (total signal/ms.mm^2)].

Following the same procedures, HT29 mouse xenografts were also be used, which express FAP on the stromal fibroblasts instead of cancer cells.[23, 25] After taking the in vivo images, the HT29 tumor was taken out and undergone microscopic study as described below.

Ex Vivo Validation Studies

After in vivo imaging studies, the animals were euthanized at 24 hour post-injection. Tumors were harvested and subjected to the following assays.

(A) Western Blot Analysis—Protein was extracted from snap frozen tumor tissue by homogenizing tissue fragments in an ice-cold lysis buffer (50 mM HEPES pH 8.0, 10% glycerol, 0.5% Triton X-100, 150 mM NaCl, 2 mM EGTA, 1.5 mM $MgCl_2$, supplemented with 10 μg/ml leupeptin, 10 μg/ml aprotinin, 100 μg/ml phenylmethylsulfonyl fluoride and 1 mM sodium orthovanadate) for 30 sec. All lysates were centrifuged at 14000 rpm for 10 min, and the supernatant stored at −70°C prior to subsequent analyses. To perform immunoblotting, lysates containing 30 μg of protein were resolved on an SDS-polyacrylamide gel (PAGE) and transferred onto polyvinylidene difluoride (PVDF) or nitrocellulose membrane. Membranes were blocked with TRIS buffered saline (TBS) containing 1% Roche blocking reagent (Roche). The membrane was incubated with primary antibody (rabbit anti-mouse FAP, 6E1) (1:1000 dilution) overnight at 4°C in blocking solution. Membranes were washed 3 times for 5 min each in TBS containing 0.1% Tween 20, and incubated with secondary HRP-linked anti-rabbit antibody for 1 h at room temperature. Equal protein loading was confirmed by reprobing the blot with antibody against GAPDH. Proteins were visualized using enhanced chemiluminescence (ECL) reagents (Roche-Boehringer Mannheim) and Typhoon 9410 Variable Mode Imager (Amersham).

(B) Confocal Microscopic and Immunohistochemistry Studies—HEK-mFAP and HEK-Vector tumors from nude mice were snap-frozen in liquid nitrogen and stored at −70°C. Frozen sections of 10 micron thickness were cut on a Leica CM3050S cryostat. The slides were taken out at room temperature for 5 min and then they were immersed into PBS for another 5 min. The slides were dried and 4 μL of mounting solution with DAPI was added. The sections were covered by a cover slide and subjected to microscopic study. Parts of frozen sections were stained with hematoxylin and eosin (H&E staining) for immunohistochemistry studies.

(C) HPLC-MS studies—The excised HEK-mFAP and HEK-Vector tumors were homogenized and extracted with DMSO. After centrifuging, tumor extracts were subjected to HPLC-MS analysis following the general HPLC methods described earlier.

In Vitro Photocytotoxicity Studies

Approximately 2.5×10^4 cells per well (200 μL) were seeded in Nunc® Lab-TekII®-CC2 96-multiwell plates and incubated for 2 days at 37°C under 5% CO_2. FAP-PPB (25 nmol), 2D-FAP-PPB (25 nmol), and FAP-PP (10 nmol) were first dissolved in 15μL of DMSO and 3μL of Tween 80. The solution was diluted with DMEM (without FBS) to 8 μM or 4 μM. After 2 days, the cells were incubated with 100 μL of these PPB solutions for 24 h at 37°C under 5% CO_2. The cells were then rinsed with PBS and refed with 150μL of the same medium before illumination. The light source consisted of a 670 ± 5 nm (0.3 W) continuous-wave pigtail laser diode system (Intense HPD). The fluence rate was 130 mW cm^{-2}. An illumination of 16 sec led to a total fluence of 2 J cm^{-2}.

Cell viability was determined by means of the colorimetric MTT assay.[37] After illumination, the cells were incubated at 37°C under 5% CO_2 overnight. The medium was removed and 3-(4,5-dimethylthiazol-2-yl)-2,5-diphenyltetrazolium bromide (Invitrogen) solution in medium (3 mg mL^{-1}, 50μL) was added to each well followed by incubation for 2 h under the same environment. A solution of sodium dodecyl sulfate in 0.1 M HCl (10% by weight, 100μL) was then added to each well. The plate was incubated in an oven at 60°C for 30 min, and then 80μL of iso-propanol was added to each well. The plate was agitated on a Spectra Max Plus microplate reader (Molecular Devices Corporation) for 5 sec before the absorbance at 570 nm at each well was taken.

Results

Design and Preparation of FAP-PPB and its Controls FAP-PP and 2D-FAP-PPB

We designed the first prototype FAP-triggered photodynamic molecular beacon based on the following principles: 1) *FAP-specific linker*: a short peptide sequence, TSGP-NQEQK with the cleavage site between Pro and Asn, was selected because FAP cleaves this peptide sequence based on the FAP-specific cleavage site in α_2-antiplasmin and its fluorogenic substrate has been used to characterize FAP's endopeptidase specificity in solutions.[17] 2) *Pyro as the photosensitizer (PS):* Pyro was selected because of its near-infrared fluorescent emissions (670 nm and 720 nm), excellent $^1O_2$ quantum yield, and its ability to deliver peptides or oligonucleotides into cancer cells.[38, 39] More importantly, its clinical potential has been demonstrated by the encouraging results for one of its analogs, Photochlor.[40] 3) *BHQ3 as the quencher:* BHQ3 functions as a dark quencher capable of efficiently quenching both Pyro's fluorescence and $^1O_2$.[32] Based on this design, we have synthesized the Pyro-TSGPNQEQK (BHQ3) (FAP-PPB) following the synthetic scheme shown in Figure 1A. Firstly, the peptide sequence **1** was synthesized following the Fmoc solid phase peptide synthesis (SPPS) protocol using a PS3™ peptide synthesizer. The Fmoc protecting group was then removed by 20% piperidine in DMF and the Pyro was conjugated to the N-terminal of peptide. The Pyro-peptide **2** was then treated with 3% TFA to remove the Mtt protecting group at the lysine allowing the subsequent coupling with BHQ3. Finally, all the remaining protecting groups on the peptide were removed by TFA with 5% Tis. The final product was purified by HPLC and characterized by UV-Vis spectroscopy and ESI mass spectrometry (*m/z* calcd for $C_{105}H_{131}N_{24}O_{19}$ $[M]^+$ 2033.3, found: 1016.9 $[M]^{2+}$). The HPLC chromatogram and the absorption and mass spectra of FAP-PPB are shown in Figure 1B-D. Following similar protocols, two controls including the quencher-less FAP-PP as the positive control and the 2D-FAP-PPB as the FAP non-cleavable control were synthesized. The latter, which had its amino acids at the cleavage site (Pro and Asn), was replaced with the corresponding D-amino acids to resist the FAP-specific cleavage. The main variation of the synthetic protocol for 2D-FAP-PPB is that the coupling reaction time for the D-amino acids was longer (3 h vs. 1 h). The characterization spectra of 2D-FAP-PPB are given in the Supporting Information (Figure S1).

Quenching Efficiency of FAP-PPB

The fluorescence intensity of FAP-PP with different concentrations of free BHQ3 and the intact FAP-PPB in DMSO and FAP buffer solutions was compared (Supporting Information, Figure S2). Increasing the ratio of external quencher BHQ3 to FAP-PP led to the decreased FAP-PP fluorescence and this effect was more prominent in the buffer solution than in DMSO. However, the quenching efficiency of external BHQ3 is much lower than that in FAP-PPB, in which BHQ3 is covalently linked. About 98% of fluorescence emission was quenched in FAP-PPB in both solutions. The quenching data of FAP-PP by free BHQ3 was further analyzed using the Stern-Volmer equation and the Stern-Volmer plots for both solutions as given in Figure S3 (Supporting Information). In DMSO, the Stern-Volmer plot has a linear relationship giving a high quenching constant ($K_{SV} = 5.3 \times 10^4$ $mol^{-1}dm^3$), validating the choice of BHQ3

as an excellent quencher for Pyro fluorescence. However, in the buffer solution, the plot shows an upward curvature suggesting that the Pyro's fluorescence is quenched by both dynamic and static quenching mechanisms.

Validation of FAP-triggered Cleavage of FAP-PPB

To evaluate the specificity of FAP-PPB toward FAP, the interactions of FAP-PPB and the negative control 2D-FAP-PPB with human FAP and murine FAP (mFAP) were first studied in a buffer solution at 37°C by fluorescence spectroscopy. mFAP was included in our studies to demonstrate a robustness of the results as it shares an 89% amino acid sequence identity with human FAP including a perfectly conserved catalytic triad.[14, 41] In addition, mFAP transfected cancer cells and mouse xenografts have been well established as useful models for the studies of FAP enzymatic activity and its role in tumor growth as well as the therapeutic property of FAP inhibitors.[22, 23] FAP-PPB showed an increase in Pyro fluorescence upon addition of either human FAP or mFAP (2 mol%), while no noticeable fluorescence increase was observed with 2D-FAP-PPB (Figure 2A). Complete cleavage of FAP-PPB by mFAP resulted in a 200-fold fluorescence increase with a complete fluorescence restoration (i.e. the final fluorescence intensity was the same as that of a 1:1 molar ratio mixture of FAP-PP and free BHQ3). The results clearly suggest that both human FAP and mFAP are able to cleave the peptide linkage of FAP-PPB with similar enzymatic activity, and at the site between Pro and Asn. The cleavage rate of FAP-PPB by mFAP was quantitatively monitored by HPLC. The cleavage process was completed in 4 h. Figure 2B shows the HPLC profile of FAP-PPB after 1 h incubation with mFAP. Two fragments peaks at 17.97 min and at 2.42 min were identified as the Pyro-containing fragment, Pyro-TSGP-COOH and the BHQ3-containing fragment, NQEQK-BHQ3, respectively. This result was based on their characteristic absorptions (Pyro: Soret band at 414 nm, BHQ3: broad peak around 658 nm) and mass spectroscopic analysis (*m/z* calcd for Pyro-TSGP-COOH $[M]^+$ 877.00, found: 877.68). Similar HPLC results were obtained with cleavage of FAP-PPB by human FAP. To the best of our knowledge, this is the first report of a direct comparison of the enzymatic activities of human FAP and mFAP in solution, suggesting mFAP is a valid model of human FAP for studying the FAP-PPB activation in vitro and in vivo.

To further examine the specificity of FAP-PPB toward FAP, FAP-PPB was incubated with dipeptidyl peptidase IV (DPPIV), which belongs to the same prolyl oligopeptidase family as FAP and is capable of cleaving N-terminal dipeptides after a proline residue. DPPIV has a 48% amino acid identity with FAP and is widely expressed in normal tissues.[12] No significant increase in fluorescence intensity was observed over 2 h and HPLC analysis showed only a single peak corresponding to the intact FAP-PPB (Figure S4 in the Supporting Information). In addition to DPPIV, a series of matrix metalloproteinases (MMPs) were also used to screen the specificity of FAP-PPB. MMPs play an important role in various physiological and pathological processes such as angiogenesis, tissue remodeling, cancer growth, and metastasis.[42–44] Furthermore, many MMPs share similar biological and proteolytic functions as FAP. In particular, MMP1, MMP8, and MMP13 are collagenases, while MMP2 and MMP9 are gelatinases.[42] Different MMPs (including MMP 1, 2, 3, 7, 8, 9, 10, 11, 12, and 13) were incubated with FAP-PPB over 16 h followed by HPLC analysis. The results, as shown in Figure S5 in the Supporting Information, showed that none of MMPs tested can cleave FAP-PPB. All these data together suggest that FAP-PPB is highly specific to FAP.

Recently, Lee et al. had reported that antiplasmin-cleaving enzyme (APCE) is a soluble form of FAP. Both proteins have the same molecular weight and enzymatic activity, and can cleave the Pro-Asn bond of met-α_2 antiplasmin.[17] Since APCE is present to some degree in blood, the stability of FAP-PPB in plasma and serum was also examined. After 24 h incubation with

either plasma or serum, it was found that only about 20% of FAP-PPB was cleaved (data not shown), demonstrating the relative serum stability of FAP-PPB allowing for its use in vivo.

Kinetic Studies for the FAP-PPB Cleavage by mFAP

To investigate the catalytic kinetics of mFAP toward FAP-PPB, different concentrations of FAP-PPB were incubated with a constant amount of mFAP. The fluorescence intensities were monitored continuously and their initial rates were measured. Figure 2D plots the initial rates versus the concentrations of FAP-PPB. Using the standard Michaelis-Menten kinetic analysis, the maximum enzymatic rate (V_{max}) and the Michaelis constant (K_m) were found to be 36 ± 2 pmol min^{-1} and 1.0 ± 0.1 μM, respectively. The latter value is comparable with that for a similar substrate, which has a sulfonyl naphthyl fluorophore (EDANS) and an azobenzene (Dabcyl) acceptor linked with the same peptide sequence.[18] This suggests that the incorporation of bulky Pyro and BHQ3 do not significantly affect the binding affinity of FAP to the peptide sequence. The catalytic constant (k_{cat}), defined as the number of catalytic events per minute per enzyme molecule, was determined to be 1.75 min^{-1} and the specificity constant (k_{cat}/K_m) was found to be 1.75×10^6 M^{-1} min^{-1}.

Validation of FAP-Specific Activation of FAP-PPB in Cancer Cells

To further examine the activation of the beacon in cancer cells, we transfected murine FAP in human embryonic kidney cells (HEK293), which were chosen for the study due to their modest tumor growth rate and their ability to readily express transfected mammalian proteins. Confocal fluorescence microscopic studies were performed on two different cell lines, namely HEK-mFAP (FAP^+) and HEK-Vector (FAP^-) cells, which were incubated with FAP-PPB or the control 2D-FAP-PPB for 6 h (Figure 3A). As anticipated, FAP-PPB showed a bright intracellular fluorescence signal in HEK-mFAP cells (Figure 3A-1), while a minimal fluorescence signal was observed in HEK-Vector cells (Figure 3A-2). When 2D-FAP-PPB was used instead, no significant fluorescence was observed in both cell lines (Figure 3A-3 and 3A-4).

After incubation, the culture media was analyzed by HPLC-MS. In media from HEK-mFAP incubated with FAP-PPB, two peaks corresponding to fragments Pyro-TSGP and NQEQK-BHQ3 were identified, whereas no cleavage was observed for the 2D-FAP-PPB under the same experimental conditions. These observations confirmed that FAP-PPB is cleaved specifically by FAP-expressing cancer cells.

To quantify the fluorescence intensity of FAP-PPB in HEK-mFAP and HEK-Vector cells, flow cytometric studies was performed at different incubation times. The distributions and the shapes of the cells are largely homogeneous after incubation with FAP-PPB, suggesting that FAP-PPB does not have dark toxicity to both cell lines. As shown in Figure 3B, the intensity in HEK-mFAP cells at all the incubation time points (1 to 24 h) is much stronger than that in the non-FAP-expressing HEK-Vector cells. For example, the fluorescence intensity in HEK-mFAP cells is about 8-fold and 13-fold compared to HEK-Vector cells at 1 h and 24 h incubation, respectively (Figure 3C). This confirms that the Pyro fluorescence can only be detected in FAP-expressing cells but not in FAP-negative cells, suggesting FAP-PPB is a useful tool for imaging FAP expression in cancers. We also examined the percentage of cleaved FAP-PPB remained in the media after incubation with HEK-mFAP cells at different time points. As expected, the longer the incubation time, the greater the amount of FAP-PPB was cleaved. After 24 h incubation, approximately 70% of FAP-PPB was cleaved giving a strong fluorescence signal (data not shown).

Validation of Activation of FAP-PPB in vivo

To evaluate the specificity of FAP-PPB in vivo, nude mice bearing HEK-mFAP tumors on their left flank and HEK-Vector tumors on their right flank were injected with 25 nmol FAP-PPB directly into the tumors and were monitored continuously by in vivo fluorescence imaging. Once FAP-PPB was injected, selective localization of fluorescence could be detected immediately in the HEK-mFAP tumor while a very low level of fluorescence was seen in the HEK-Vector tumor (Figure 4A). The fluorescence signals on both tumors were steady for the first 7 h indicating that the activation of FAP-PPB was accomplished relatively quickly (within 5 min). After 24 h, the fluorescence signal in both tumors increased, but the signal in the HEK-Vector tumor was significantly lower (about half) than that in the HEK-mFAP tumor (based on the numerical data of fluorescence intensity per exposure time at the tumor site). The Western blot of tumors extracted 24 h post-injection showed that FAP was highly expressed in HEK-mFAP tumor while it was absent in HEK-Vector tumor (Figure 4B). After homogenizing the tumors followed by extraction with DMSO, the extracted filtrates were analyzed by HPLC-MS. The results showed that FAP-PPB was cleaved in the HEK-mFAP tumor at the FAP specific cleavage site, generating the two fragments Pyro-TSGP and NQEQK-BHQ3 (Figure 4C), whereas no cleavage was observed in the HEK-Vector tumor. In addition, confocal microscopic studies of frozen sections of tumor tissue at 10 micron showed a strong Pyro's fluorescence signal within the cytoplasm of cancer cells and fibroblasts in the HEK-mFAP tumors, while only a very weak signal was observed in the HEK-Vector tumor section (Figure 4D). All these data confirmed that FAP-PPB can be cleaved selectively and specifically in FAP-rich tumors in vivo.

To further validate the in vivo FAP-specificity of FAP-PPB, a nude mouse bearing two HEK-mFAP (FAP^+) tumors was directly injected with FAP-PPB on the left flank and 2D-FAP-PPB on the right flank, and their in vivo images were monitored over 8 h. As shown in Figure 5, immediately after the injection, the tumor injected with FAP-PPB showed an intense fluorescence signal while no fluorescence signal was detected in the tumor injected with 2D-FAP-PPB. HPLC analysis of tumor extracts 24h post-injection showed that FAP-PPB was cleaved specifically while little non-specific cleavages were observed in 2D-FAP-PPB.

In order to confirm the in vivo activation of FAP-PPB by FAP-expressing stromal fibroblasts, a nude mouse bearing HT29 tumor (colorectal cancer) on the left flank was used for comparison because of the abundant FAP expression in the stroma of human colorectal carcinomas.[23, 25] As shown in Figure 6A, once the FAP-PPB was directly injected to the HT29 tumor, strong fluorescence signal was observed immediately and it lasted for 24 h. Furthermore, confocal microscopic studies of HT29 tumor frozen section tissue showed bright Pyro's fluorescence signals within both cancer cells and fibroblasts (Figure 6B). It suggests that the FAP-PPB can also be cleaved on the stroma and then the Pyro-peptide fragments diffused to the adjacent cancer cells (reverse situation of HEK-mFAP xenograft). These data strongly supported that FAP-PPB can be cleaved selectively and specifically in FAP-rich tumors (either on stroma or cancer cells) in vivo.

Photocytotoxicity Assay of FAP-PPB

In addition to the diagnostic utility of this beacon, we also evaluated its therapeutic potential. The cell viability of HEK-mFAP and HEK-Vector cells treated with FAP-PPB, FAP-PP and 2D-FAP-PPB were investigated in the absence or presence of light (Figure 7). Firstly, the formulation that we used (DMSO and Tween 80) is non-toxic to the cells. FAP-PP, which acted as a positive control, could kill both cell lines in the presence of light, while the FAP non-cleavable control 2D-FAP-PPB was essentially non-cytotoxic. Importantly, FAP-PPB was non-cytotoxic in the absence of light, but showed significant photocytotoxicity in FAP-expressing cells but not in the HEK-Vector cells. With 2 J cm^{-2} of light dose, 8 μM of FAP-

PPB reduced the viability to 55%, which was slightly greater than that of 4 μM positive control FAP-PP (40%). The PDT efficacy of FAP-PPB cannot be fully restored possibly because only about 70% of FAP-PPB was cleaved after 24 h incubation in HEK-mFAP cells. This preliminary study clearly shows that our photodynamic molecular beacon FAP-PPB is potentially useful for selective treatment of epithelial cancers.

Discussion

We have successfully synthesized a new photodynamic molecular beacon (FAP-PPB) which is highly specific toward both human FAP and mFAP, but not other proteases including DPPIV and a variety of MMPs. In vitro studies confirmed unequivocally its FAP-specific activation. For in vivo studies, intratumor injection of FAP-PPB directly into the FAP-expressing tumor showed a rapid activation and strong fluorescence signal within 5 min post-injection. HPLC analysis of tumor extract at 24 h post-injection confirmed that the beacon activation is mostly FAP-specific. In addition, preliminary PDT studies demonstrated that FAP-PPB's photocytotoxicity is also FAP-specific. Therefore, this FAP-PPB may serve as both a tumor specific diagnostic agent and a directed PDT agent.

There are a number of additional advantages to the FAP-triggered photodynamic molecular beacon approach. After being liberated extracellularly from the FAP-PPB by FAP cleavage, the Pyro-peptide fragment rapidly enters cells at the site of activation because of the high degree of lipophilicity and cell penetrating ability of the Pyro moiety,[32] with little release into the general circulation, thus minimizing distant side effects. This mechanism is supported by our ex vivo experiments (confocal microscopic study and H&E staining) showing that once the FAP-PPB is cleaved by the FAP in HEK-mFAP xenografts, the Pyro-peptide fragment is retained at the site of tumor and distributes evenly in both the cancer cells and fibroblasts. Hence, PDT treatment on the tumor might initiate cytotoxicity of both the cancer cells and the surrounding fibroblasts, irrespective of whether the FAP-PPB is cleaved by FAP on the cancer cell (e.g. sarcoma), or on the CAFs of epithelial cancers. Such multicell-targeted cytotoxicity may further interrupt the signaling between fibroblasts and the adjacent cancer cells, resulting in synergistic cytotoxic effects.

One possible limitation of using FAP-PPB for epithelial cancer detection and treatment is no selective accumulation of FAP-PPB at the tumor site after the intravenous tail-vein injection. This is not surprising as limited delivery efficiency following systematic administration is a common hurdle for many small molecule therapeutics. Recent advances in cancer nanotechnology might offer potential solutions to address this issue.[45] For example, a large number of FAP-PPB molecules can be encapsulated in single nanoparticles to shield them from circulation and to release them in a controlled manner into the extracellular tumor microenvironment through the passive enhanced permeability and retention effect.[46] An alternative approach is to use a tumor-targeting peptide to augment the local accumulation of FAP-PPB at the tumor sites. For example, Scheeren *et al.* has utilized a RGD peptide for targeting a plasmin-cleavable doxorubicin prodrug to the integrin receptors on tumor neovasculature.[47] Their approach has led to a synergistic effect in which both peptides act together to release active drug at the tumor site. We believe this approach could be adapted for the enhanced delivery of our FAP-PPB to the tumor microenvironment. In another alternative, Tsien *et al.* have introduced a new strategy for selectively delivering molecules to tumor cells based on protease-triggered local 'unleashing' of cell-penetrating peptides.[48] The electrostatic attraction of such polycationic peptides with polyanionic peptides blocks their cell entry until the protease-mediated cleavage of the linker. We envision that this approach could be adapted to our FAP-PPB to accelerate cell entry speed of the Pyro-peptide fragment following the beacon activation, thus further delineating the margins between malignant and normal tissues.

Conclusion

A novel FAP-triggered photodynamic molecular beacon (FAP-PPB) has been successfully synthesized and characterized. It can be effectively cleaved by human FAP and mFAP in a specific manner with similar enzymatic activities. As revealed by flow cytometry and confocal microscopy, the probe can be activated in FAP-transfected cancer cells, but remains silent in FAP-negative cells. The activation of FAP-PPB has also been validated in vivo using HEK-mFAP and HEK-Vector xenografts. All the results show that FAP-PPB is highly specific to FAP and can serve as an excellent fluorescent probe for the detection of FAP, both in vitro and in vivo. In addition, FAP-PPB is photocytotoxic toward HEK-mFAP cells while it remains essentially non-cytotoxic toward FAP-negative HEK-Vector cells. Therefore, this newly developed photodynamic molecular beacon is not only a specific probe for the diagnosis of FAP-expressing epithelial cancers, but also a promising therapeutic agent for this kind of cancers. We envision that FAP-PPB may be potentially useful for fluorescence-guided surgery allowing completeness of resection by “extending the surgeon’s vision” and/or with adjuvant PDT treatment to safely and effectively eradicate any post-resection residual tumor cells and eliminate microscopic deposits.

Supplementary Material

Refer to Web version on PubMed Central for supplementary material.

Acknowledgments

This study was conducted with the support of the Canadian Institute of Health Research (#179821), the Ontario Institute for Cancer Research through funding provided by the Government of Ontario, and the Joey and Toby Tanenbaum/ Brazilian Ball Chair in Prostate Cancer Research.

Abbreviations

BHQ3	black hole quencher 3
CAFs	cancer-associated fibroblasts
DAPI	4′,6-diamidino-2-phenylinodole
DIPEA	*N*,*N*-diisopropylethylamine
DMF	*N*,*N*-dimethylformamide
DMSO	dimethyl sulfoxide
ESI	electrospray ionization
FAP	fibroblast activation protein
FAP-PPB	fibroblast activation protein triggered photodynamic molecular beacon
Fmoc	9H-fluoren-9-ylmethoxycarbonyl
HBTU	o-(benzotriazol-1-yl)-*N*,*N*,*N*′,*N*′-tetramethyluronium hexafluorophosphate
HOBt	1-hydroxybenzotriazole
mFAP	murine fibroblast activation protein
PDT	photodynamic therapy

PS	photosensitizer
Pyro	Pyropheophorbide *a*
TFA	trifluoroacetic acid
Tis	triisopropylsilane
Q	quencher

References

1. Haslam SZ, Woodward TL. Host microenvironment in breast cancer development: epithelial-cell-stromal-cell interactions and steroid hormone action in normal and cancerous mammary gland. Breast Cancer Res 2003;5:208–215. [PubMed: 12817994]
2. Iozzo RV. Tumor stroma as a regulator of neoplastic behavior. Agonistic and antagonistic elements embedded in the same connective tissue. Lab Invest 1995;73:157–160. [PubMed: 7637316]
3. Ronnov-Jessen L, Petersen OW, Bissell MJ. Cellular changes involved in conversion of normal to malignant breast: importance of the stromal reaction. Physiol Rev 1996;76:69–125. [PubMed: 8592733]
4. Zigrino P, Loffek S, Mauch C. Tumor-stroma interactions: their role in the control of tumor cell invasion. Biochimie 2005;87:321–328. [PubMed: 15781319]
5. Kalluri R, Zeisberg M. Fibroblasts in cancer. Nat Rev Cancer 2006;6:392–401. [PubMed: 16572188]
6. Bhowmick NA, Neilson EG, Moses HL. Stromal fibroblasts in cancer initiation and progression. Nature 2004;432:332–337. [PubMed: 15549095]
7. Micke P, Ostman A. Tumour-stroma interaction: cancer-associated fibroblasts as novel targets in anti-cancer therapy? Lung Cancer 2004;45(Suppl 2):S163–175. [PubMed: 15552797]
8. Orimo A, Gupta PB, Sgroi DC, Arenzana-Seisdedos F, Delaunay T, Naeem R, Carey VJ, Richardson AL, Weinberg RA. Stromal fibroblasts present in invasive human breast carcinomas promote tumor growth and angiogenesis through elevated SDF-1/CXCL12 secretion. Cell 2005;121:335–348. [PubMed: 15882617]
9. Olumi AF, Grossfeld GD, Hayward SW, Carroll PR, Tlsty TD, Cunha GR. Carcinoma-associated fibroblasts direct tumor progression of initiated human prostatic epithelium. Cancer Res 1999;59:5002–5011. [PubMed: 10519415]
10. Garin-Chesa P, Old LJ, Rettig WJ. Cell surface glycoprotein of reactive stromal fibroblasts as a potential antibody target in human epithelial cancers. Proc Natl Acad Sci U S A 1990;87:7235–7239. [PubMed: 2402505]
11. Rettig WJ, Garin-Chesa P, Beresford HR, Oettgen HF, Melamed MR, Old LJ. Cell-surface glycoproteins of human sarcomas: differential expression in normal and malignant tissues and cultured cells. Proc Natl Acad Sci U S A 1988;85:3110–3114. [PubMed: 2896356]
12. Scanlan MJ, Raj BK, Calvo B, Garin-Chesa P, Sanz-Moncasi MP, Healey JH, Old LJ, Rettig WJ. Molecular cloning of fibroblast activation protein alpha, a member of the serine protease family selectively expressed in stromal fibroblasts of epithelial cancers. Proc Natl Acad Sci U S A 1994;91:5657–5661. [PubMed: 7911242]
13. Park JE, Lenter MC, Zimmermann RN, Garin-Chesa P, Old LJ, Rettig WJ. Fibroblast activation protein, a dual specificity serine protease expressed in reactive human tumor stromal fibroblasts. J Biol Chem 1999;274:36505–36512. [PubMed: 10593948]
14. Niedermeyer J, Enenkel B, Park JE, Lenter M, Rettig WJ, Damm K, Schnapp A. Mouse fibroblast-activation protein--conserved Fap gene organization and biochemical function as a serine protease. Eur J Biochem 1998;254:650–654. [PubMed: 9688278]
15. Christiansen VJ, Jackson KW, Lee KN, McKee PA. Effect of fibroblast activation protein and alpha2-antiplasmin cleaving enzyme on collagen types I, III, and IV. Arch Biochem Biophys 2007;457:177–186. [PubMed: 17174263]

16. Kelly T. Fibroblast activation protein-alpha and dipeptidyl peptidase IV (CD26): cell-surface proteases that activate cell signaling and are potential targets for cancer therapy. Drug Resist Updat 2005;8:51–58. [PubMed: 15939342]

17. Lee KN, Jackson KW, Christiansen VJ, Lee CS, Chun JG, McKee PA. Antiplasmin-cleaving enzyme is a soluble form of fibroblast activation protein. Blood 2006;107:1397–1404. [PubMed: 16223769]

18. Edosada CY, Quan C, Tran T, Pham V, Wiesmann C, Fairbrother W, Wolf BB. Peptide substrate profiling defines fibroblast activation protein as an endopeptidase of strict Gly(2)-Pro(1)-cleaving specificity. FEBS Lett 2006;580:1581–1586. [PubMed: 16480718]

19. Aggarwal S, Brennen WN, Kole TP, Schneider E, Topaloglu O, Yates M, Cotter RJ, Denmeade SR. Fibroblast activation protein peptide substrates identified from human collagen I derived gelatin cleavage sites. Biochemistry 2008;47:1076–1086. [PubMed: 18095711]

20. Cheng JD, Weiner LM. Tumors and their microenvironments: tilling the soil. Commentary re: A. M. Scott et al., A Phase I dose-escalation study of sibrotuzumab in patients with advanced or metastatic fibroblast activation protein-positive cancer. Clin Cancer Res 2003;9:1639–1647. [PubMed: 12738716]Clin Cancer Res 2003;9:1590–1595. [PubMed: 12738710]

21. Henry LR, Lee HO, Lee JS, Klein-Szanto A, Watts P, Ross EA, Chen WT, Cheng JD. Clinical implications of fibroblast activation protein in patients with colon cancer. Clin Cancer Res 2007;13:1736–1741. [PubMed: 17363526]

22. Cheng JD, Valianou M, Canutescu AA, Jaffe EK, Lee HO, Wang H, Lai JH, Bachovchin WW, Weiner LM. Abrogation of fibroblast activation protein enzymatic activity attenuates tumor growth. Mol Cancer Ther 2005;4:351–360. [PubMed: 15767544]

23. Cheng JD, Dunbrack RL Jr, Valianou M, Rogatko A, Alpaugh RK, Weiner LM. Promotion of tumor growth by murine fibroblast activation protein, a serine protease, in an animal model. Cancer Res 2002;62:4767–4772. [PubMed: 12183436]

24. Scott AM, Wiseman G, Welt S, Adjei A, Lee FT, Hopkins W, Divgi CR, Hanson LH, Mitchell P, Gansen DN, Larson SM, Ingle JN, Hoffman EW, Tanswell P, Ritter G, Cohen LS, Bette P, Arvay L, Amelsberg A, Vlock D, Rettig WJ, Old LJ. A Phase I dose-escalation study of sibrotuzumab in patients with advanced or metastatic fibroblast activation protein-positive cancer. Clin Cancer Res 2003;9:1639–1647. [PubMed: 12738716]

25. Welt S, Divgi CR, Scott AM, Garin-Chesa P, Finn RD, Graham M, Carswell EA, Cohen A, Larson SM, Old LJ, et al. Antibody targeting in metastatic colon cancer: a phase I study of monoclonal antibody F19 against a cell-surface protein of reactive tumor stromal fibroblasts. J Clin Oncol 1994;12:1193–1203. [PubMed: 8201382]

26. Hofheinz RD, al-Batran SE, Hartmann F, Hartung G, Jager D, Renner C, Tanswell P, Kunz U, Amelsberg A, Kuthan H, Stehle G. Stromal antigen targeting by a humanised monoclonal antibody: an early phase II trial of sibrotuzumab in patients with metastatic colorectal cancer. Onkologie 2003;26:44–48. [PubMed: 12624517]

27. Adams S, Miller GT, Jesson MI, Watanabe T, Jones B, Wallner BP. PT-100, a small molecule dipeptidyl peptidase inhibitor, has potent antitumor effects and augments antibody-mediated cytotoxicity via a novel immune mechanism. Cancer Res 2004;64:5471–5480. [PubMed: 15289357]

28. Uprichard MJ, O'Day SJ, Pavlick AC, Richards DA, Frenette G, Stephenson J, Anthony S, Pacciucci PA, Vrhovac V, Cunningham C. Phase 2 study of talabostat and cisplatin in stage IV melanoma. Journal of Clinical Oncology 2005;23:725s.

29. Cunningham C, Pavlick AC, Khan KD, Frenette G, O'Day S, Stephenson J, Gonzalez R, Yang Z, Vrhovac V, Uprichard MJ. Phase 2 trial of talabostat and cisplatin in patients with stage IV melanoma. Journal of Clinical Oncology 2006;24:462s.

30. Redman BG, Ernstoff MS, Gajewski TF, Cunningham C, Lawson DH, Gregoire L, Haltom E, Uprichard MJ. Phase 2 trial of talabostat in stage IV melanoma. Journal of Clinical Oncology 2005;23:727s.

31. Narra K, Mullins SR, Lee HO, Strzemkowski-Brun B, Magalong K, Christiansen VJ, McKee PA, Egleston B, Cohen SJ, Weiner LM, Meropol NJ, Cheng JD. Phase II trial of single agent Val-boroPro (Talabostat) inhibiting Fibroblast Activation Protein in patients with metastatic colorectal cancer. Cancer Biol Ther 2007;6:1691–1699. [PubMed: 18032930]

32. Zheng G, Chen J, Stefflova K, Jarvi M, Li H, Wilson BC. Photodynamic molecular beacon as an activatable photosensitizer based on protease-controlled singlet oxygen quenching and activation. Proc Natl Acad Sci U S A 2007;104:8989–8994. [PubMed: 17502620]
33. Chen J, Jarvi M, Lo PC, Stefflova K, Wilson BC, Zheng G. Using the singlet oxygen scavenging property of carotenoid in photodynamic molecular beacons to minimize photodamage to non-targeted cells. Photochem Photobiol Sci 2007;6:1311–1317. [PubMed: 18046487]
34. Chan, WC.; White, PD. Fmoc solid phase peptide synthesis: a practical approach. Oxford University Press; Oxford; New York: 2000.
35. Zheng G, Li H, Zhang M, Lund-Katz S, Chance B, Glickson JD. Low-density lipoprotein reconstituted by pyropheophorbide cholesteryl oleate as target-specific photosensitizer. Bioconjug Chem 2002;13:392–396. [PubMed: 12009925]
36. Lakowicz, JR. Principles of fluorescence spectroscopy. Vol. 3. Springer; New York: 2006.
37. Tada H, Shiho O, Kuroshima K, Koyama M, Tsukamoto K. An Improved Colorimetric Assay for Interleukin-2. Journal of Immunological Methods 1986;93:157–165. [PubMed: 3490518]
38. Stefflova K, Chen J, Marotta D, Li H, Zheng G. Photodynamic therapy agent with a built-in apoptosis sensor for evaluating its own therapeutic outcome in situ. J Med Chem 2006;49:3850–3866. [PubMed: 16789741]
39. Chen J, Lovell JF, Lo PC, Stefflova K, Niedre M, Wilson BC, Zheng G. A tumor mRNA-triggered photodynamic molecular beacon based on oligonucleotide hairpin control of singlet oxygen production. Photochem Photobiol Sci 2008;7:775–781. [PubMed: 18597024]
40. Bellnier DA, Greco WR, Loewen GM, Nava H, Oseroff AR, Pandey RK, Tsuchida T, Dougherty TJ. Population pharmacokinetics of the photodynamic therapy agent 2-[1-hexyloxyethyl]-2-devinyl pyropheophorbide-a in cancer patients. Cancer Res 2003;63:1806–1813. [PubMed: 12702566]
41. Niedermeyer J, Scanlan MJ, Garin-Chesa P, Daiber C, Fiebig HH, Old LJ, Rettig WJ, Schnapp A. Mouse fibroblast activation protein: molecular cloning, alternative splicing and expression in the reactive stroma of epithelial cancers. Int J Cancer 1997;71:383–389. [PubMed: 9139873]
42. McCawley LJ, Matrisian LM. Matrix metalloproteinases: they're not just for matrix anymore! Curr Opin Cell Biol 2001;13:534–540. [PubMed: 11544020]
43. Egeblad M, Werb Z. New functions for the matrix metalloproteinases in cancer progression. Nat Rev Cancer 2002;2:161–174. [PubMed: 11990853]
44. Page-McCaw A, Ewald AJ, Werb Z. Matrix metalloproteinases and the regulation of tissue remodelling. Nat Rev Mol Cell Biol 2007;8:221–233. [PubMed: 17318226]
45. Ferrari M. Cancer nanotechnology: opportunities and challenges. Nat Rev Cancer 2005;5:161–171. [PubMed: 15738981]
46. Zhang L, Gu FX, Chan JM, Wang AZ, Langer RS, Farokhzad OC. Nanoparticles in medicine: therapeutic applications and developments. Clin Pharmacol Ther 2008;83:761–769. [PubMed: 17957183]
47. de Groot FM, Broxterman HJ, Adams HP, van Vliet A, Tesser GI, Elderkamp YW, Schraa AJ, Kok RJ, Molema G, Pinedo HM, Scheeren HW. Design, synthesis, and biological evaluation of a dual tumor-specific motive containing integrin-targeted plasmin-cleavable doxorubicin prodrug. Mol Cancer Ther 2002;1:901–911. [PubMed: 12481411]
48. Jiang T, Olson ES, Nguyen QT, Roy M, Jennings PA, Tsien RY. Tumor imaging by means of proteolytic activation of cell-penetrating peptides. Proc Natl Acad Sci U S A 2004;101:17867–17872. [PubMed: 15601762]

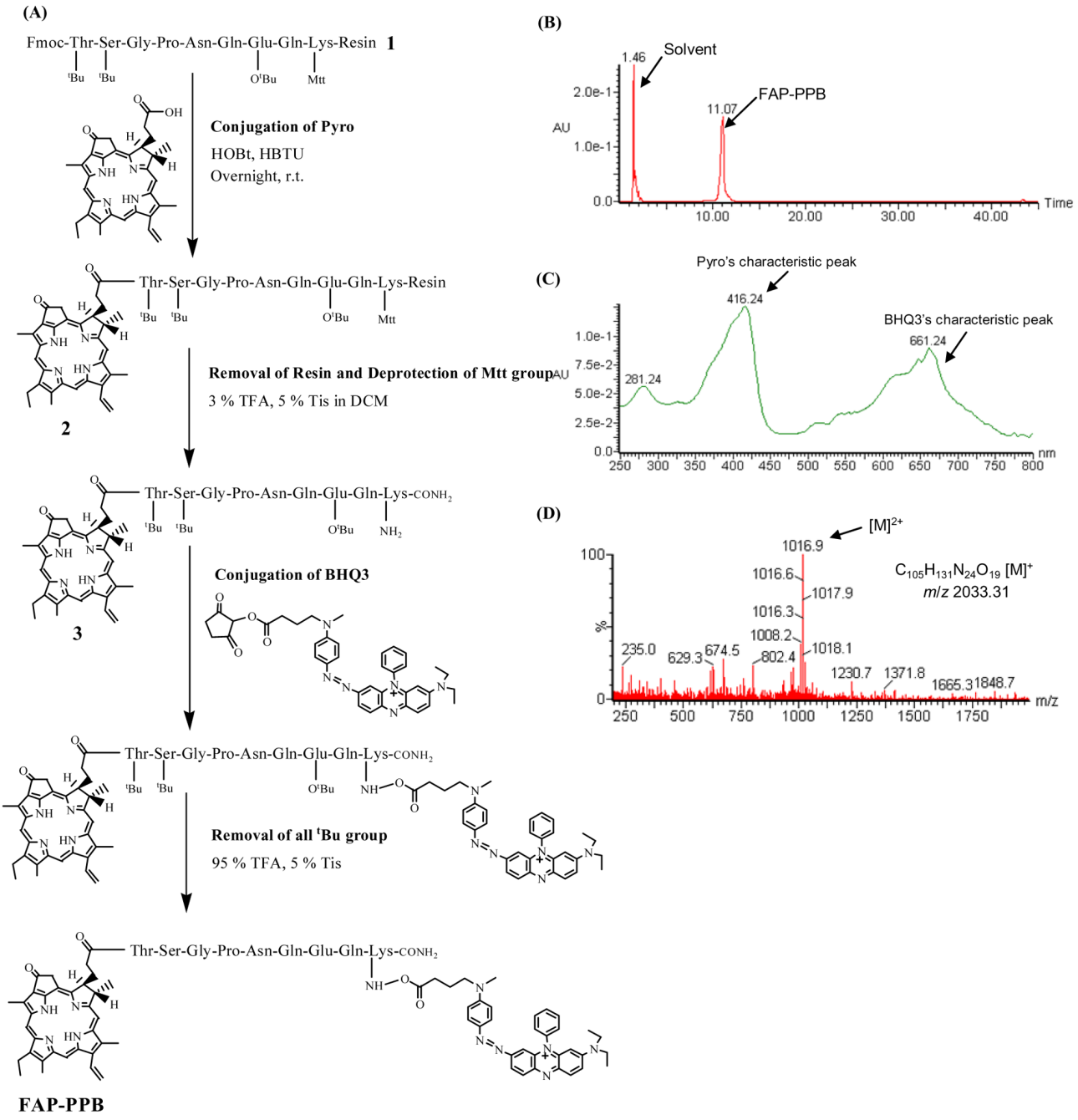

Figure 1.

Preparation and characterization of FAP-PPB. (A) Synthetic protocol. (B) HPLC chromatogram, (C) UV-Vis spectrum, and (D) ESI mass spectrum of FAP-PPB.

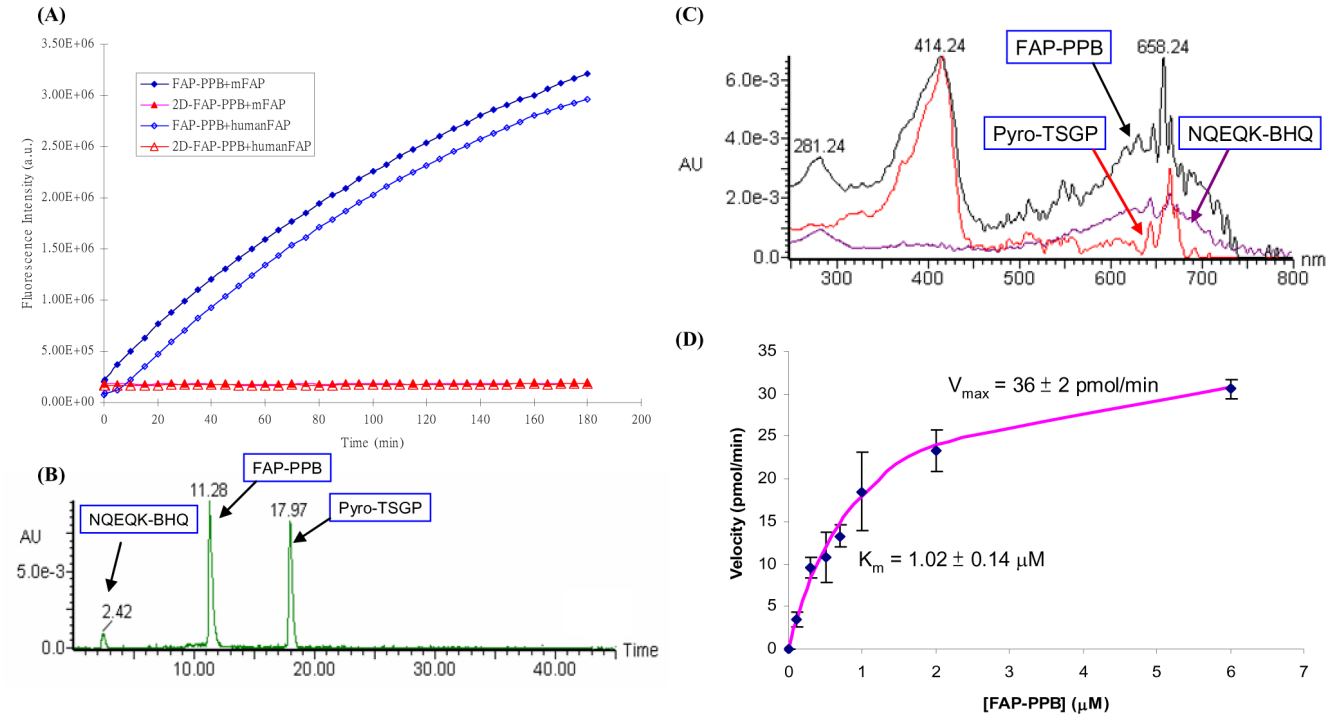

Figure 2.

(A) Changes in fluorescence intensity of FAP-PPB and 2D-FAP-PPB upon interactions with human FAP and mFAP (50:1 molar ratio) in a TRIS buffer solution at 37 °C. (B) HPLC profile of FAP-PPB after 1-hour incubation with mFAP. (C) UV-Vis spectra for the corresponding portions. (D) Variation of the initial cleavage rate of FAP-PPB by mFAP (2 μg) (as shown by the increase in fluorescence intensity at 665 nm) with increasing concentration of FAP-PPB. The estimated Km and Vmax values are indicated and the error bars represent standard deviations from the mean from triplicate measurements.

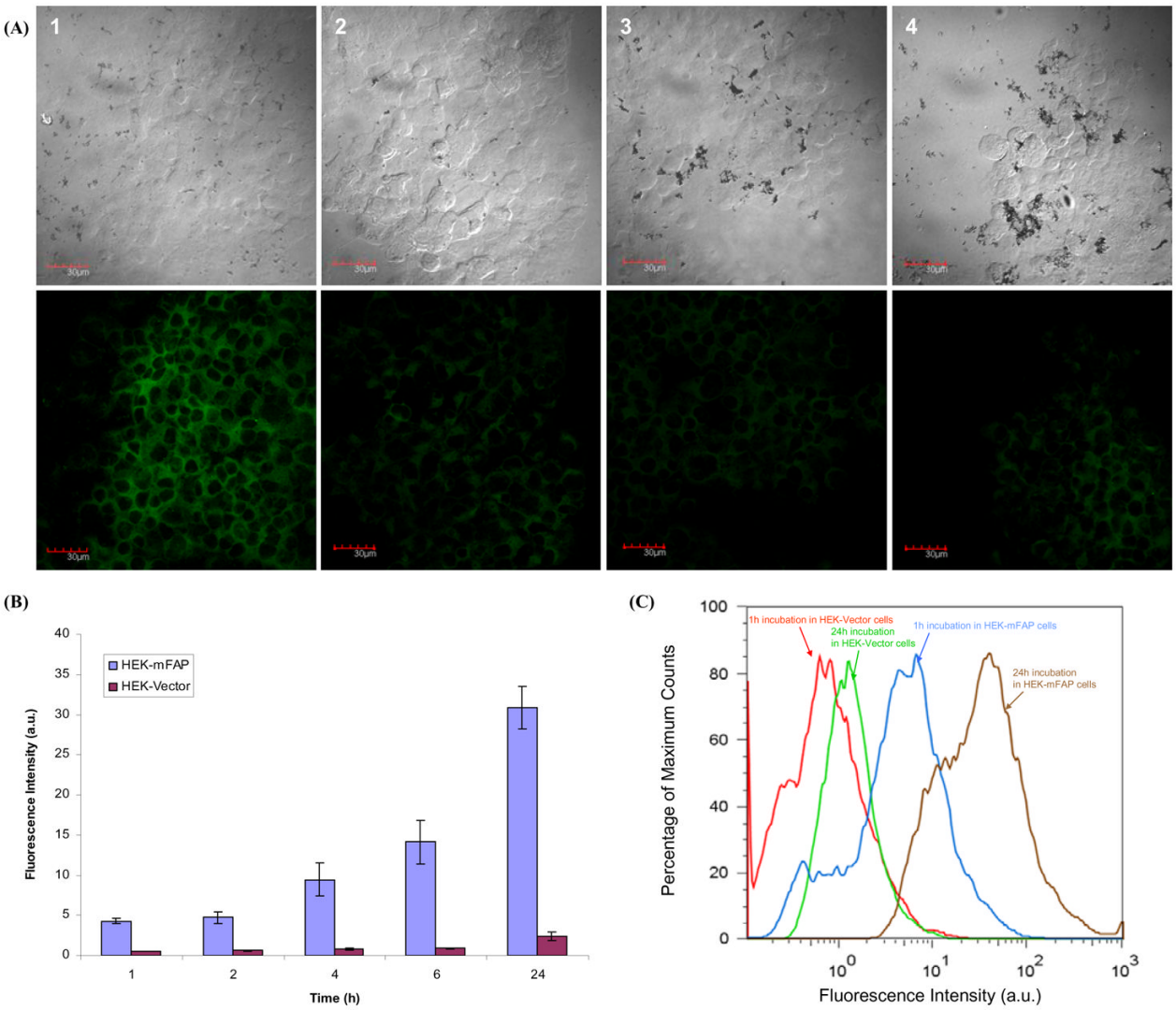

Figure 3.

(A) Confocal microscopic images of FAP-PPB and 2D-FAP-PPB (both at 25 μM) in HEK-mFAP and HEK-Vector cells showing the bright field (upper row) and fluorescence (lower row) images in each case. (1) FAB-PPB in HEK-mFAP cells, (2) FAB-PPB in HEK-Vector cells, (3) 2D-FAP-PPB in HEK-mFAP cells, and (4) 2D-FAP-PPB in HEK-Vector cells. (B) Comparison of the intracellular fluorescence intensity of FAP-PPB in HEK-mFAP and HEK-Vector cells monitored by flow cytometry. Data are expressed as mean values ± S.E.M. of three independent experiments. (C) Fluorescence histograms for HEK-mFAP and HEK-Vector cells after incubation with FAP-PPB for 1 and 24 h.

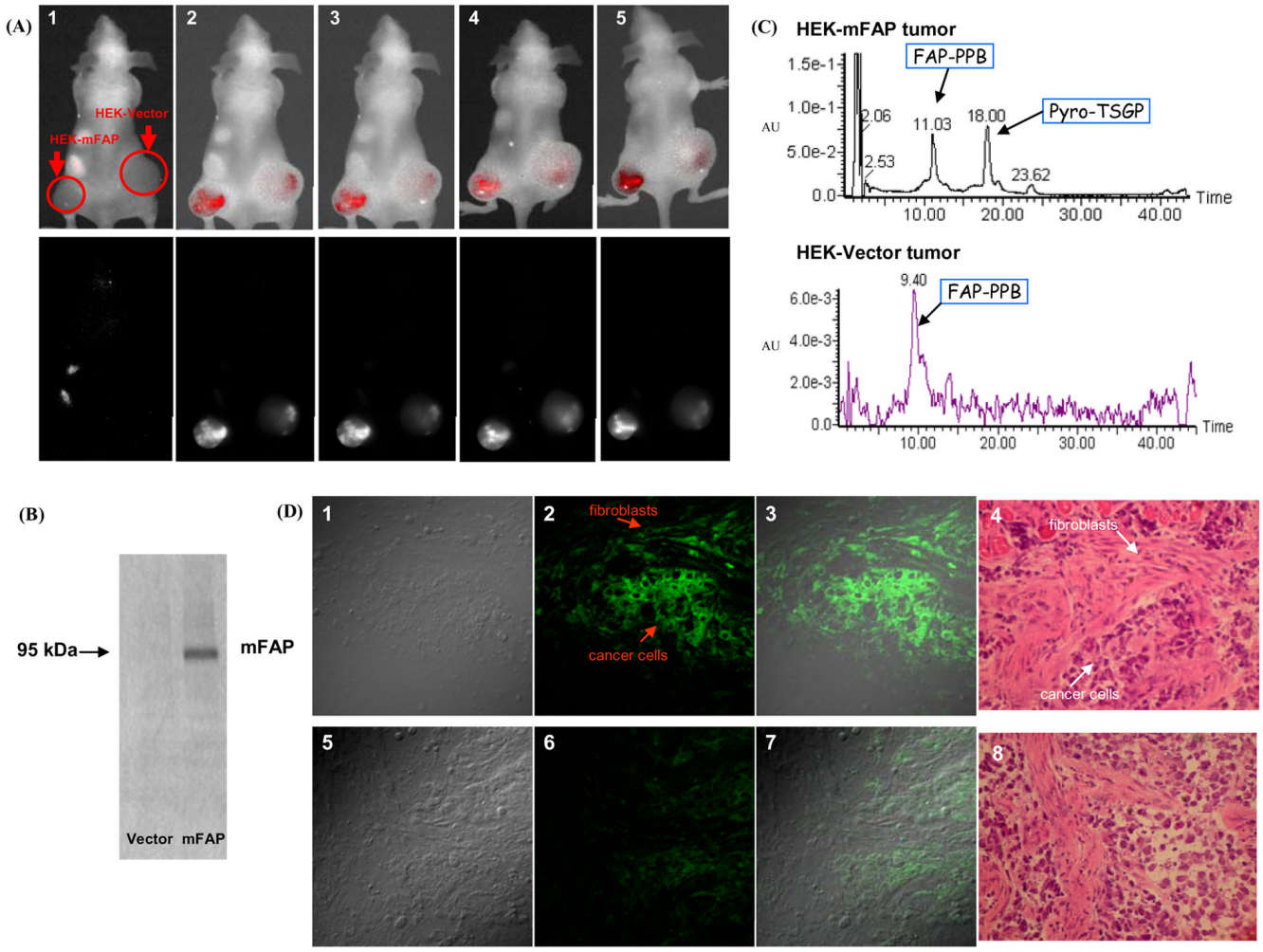

Figure 4.

(A) In vivo images of mice showing the composite fluorescence (top row) and Pyro's specific fluorescence (bottom row) before and after intra-tumor injection of FAP-PPB (25 nmol) on each side of tumor. (1) Pre-scan, (2) 5 min post injection, (3) 1h post injection, (4) 7h post injection, and (5) 24h post injection. (B) Western blot analysis of HEK-mFAP and HEK-Vector tumor tissues. (C) HPLC profile of the HEK-mFAP and the HEK-Vector tumor extracts. (D) Microscopic images showing the localization of FAP-PPB in HEK-mFAP (upper row) and HEK-Vector (lower row) tumors frozen sections. (1) and (5) Differential interference contrast images, (2) and (6) Pyro's fluorescence images, (3) and (7) Superimposed images, (4) and (8) H&E staining images.

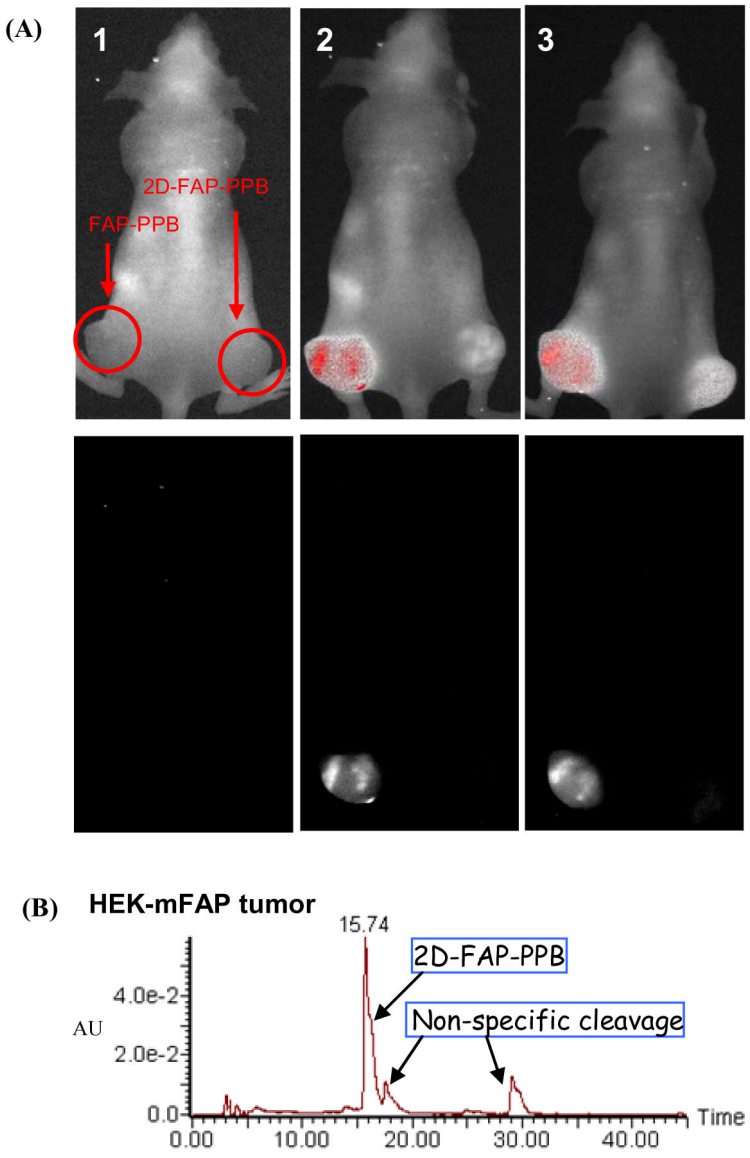

Figure 5.

(A) In vivo images of mice bearing two HEK-mFAP tumors showing the composite fluorescence (top row) and Pyro's specific fluorescence (bottom row) before and after intra-tumor injection of FAP-PPB (25 nmol) on the left side tumor and 2D-FAP-PPB on the right side tumor. (1) Pre-scan, (2) 5 min post injection, (3) 8h post injection. (B) HPLC profile of the HEK-mFAP tumor extract 24h post-injection with 2D-FAP-PPB.

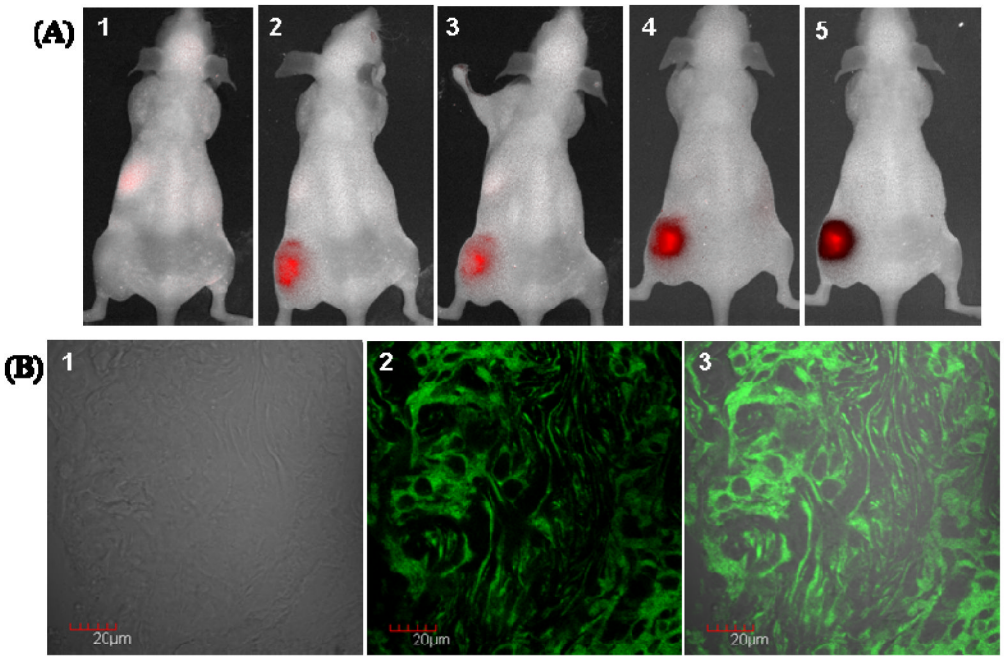

Figure 6.

(A) In vivo images of mice bearing HT29 tumor showing the composite fluorescence before and after intra-tumor injection of FAP-PPB (25 nmol) on the left flank. (1) Prescan, (2) 5 min post injection, (3) 1h post injection, (4) 8h post injection, and (5) 24h post injection. (B) Microscopic images showing the localization of FAP-PPB in HT29 tumor frozen section. (1) Differential interference contrast image, (2) Pyro's fluorescence image, and (3) Superimposed image.

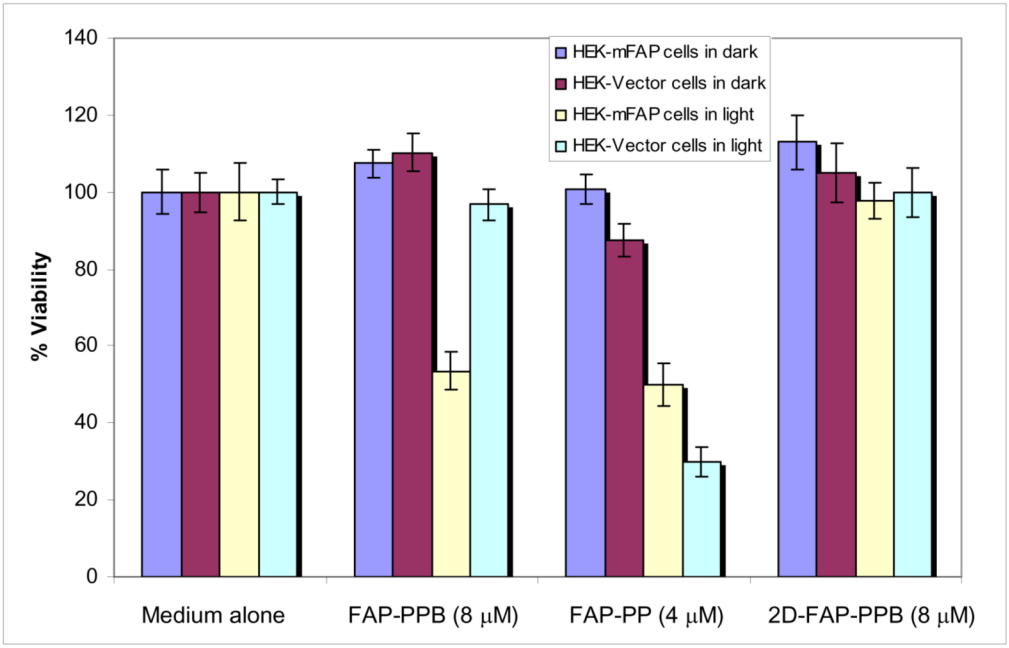

Figure 7.

Effects of FAP-PPB (8 μM), FAP-PP (4 μM) and 2D-FAP-PPB (8 μM) on HEK-mFAP and HEK-Vector cells in the absence and presence of light. For the latter, the cells were irridated with a laser (λ= 670nm ±5nm, 130 mW cm^{-2}, 2 J cm^{-2}). Data are expressed as mean values ± S.E.M. of three independent experiments, each performed in quadruplicate.